Inorg. Chem. **2003**, *42*, 7921−7931

Panchromatic Sensitization of Nanocrystalline TiO_2 with *cis*-Bis(4-carboxy-2-[2′-(4′-carboxypyridyl)]quinoline)bis(thiocyanato-*N*)ruthenium(II)

Masatoshi Yanagida, Takeshi Yamaguchi, Mitsuhiko Kurashige, Kohjiro Hara, Ryuzi Katoh, Hideki Sugihara,* and Hironori Arakawa*

Photoreaction Control Research Center, National Institute of Advanced Industrial Science and Technology, 1-1-1 Higashi, AIST-Tsukuba Central 5, Tsukuba, Ibaraki 305-8565, Japan

Received June 16, 2003

We compared the spectral (IR and Raman), electrochemical, and photoelectrochemical properties of nanocrystalline TiO_2 sensitized with the newly synthesized complex $[NBu_4]_2$[*cis*-Ru(Hdcpq)$_2$(NCS)$_2$] (**1**; $[NBu_4]^+$ = tetrabutylammonium cation; H_2dcpq = 4-carboxy-2-[2′-(4′-carboxypyridyl)]quinoline) with those of TiO_2 sensitized with $[NBu_4]_2$[*cis*-Ru(Hdcbpy)$_2$(NCS)$_2$] (**2**; H_2dcbpy = 4,4′-dicarboxy-2,2′-bipyridine) and $[NBu_4]_2$[*cis*-Ru(Hdcbiq)$_2$(NCS)$_2$] (**3**; H_2dcbiq = 4,4′-dicarboxy-2,2′-biquinoline). Complex **1** achieved efficient sensitization of nanocrystalline TiO_2 films over a wide visible and near-IR region, generating a large short-circuit photocurrent. The absorbed photon-to-current conversion efficiency decreased in the order **2** > **1** > **3** with the decrease in the free energy change ($-\Delta G_{inj}$) of the electron injection from the ruthenium complex to TiO_2. The open-circuit photovoltages (V_{oc}'s) of dye-sensitized solar cells decreased in the order **2** > **1** > **3** with the increase in the dark current resulting from reverse electron transfer from TiO_2 to I_3^-. The sensitizer-dependent V_{oc} value can be interpreted as a result of reverse electron transfer through the sensitizing dye molecules.

Introduction

Several polypyridine ruthenium(II) complexes that absorb light from the visible to the near-IR region have been synthesized and investigated with the aim of improving the solar-to-energy conversion efficiencies of solar cells based on nanocrystalline TiO_2.[1−15] To absorb light up to the near-IR region, the excited state and ground state of the sensitizer need to be tuned. The excited and ground states of the ruthenium complexes need to maintain sufficient thermodynamic driving force for the injection of electrons from the ruthenium complex in its excited state to the conduction band of TiO_2 and for the transfer of electrons from an electron donor in an electrolyte to the oxidized ruthenium complex.[3−13] The energy levels of ruthenium complexes in the excited state have been positively shifted by introducing a ligand with a low-lying π^* molecular orbital. Argazzi and co-workers have investigated solar cells based on TiO_2 sensitized with ruthenium complexes containing 5,5′-dicarboxy-2,2′-bipyridine, of which the π^* orbital is less negative in energy than that containing 4,4′-dicarboxy-2,2′-bipyridine (H_2dcbpy).[10,11] We have synthesized ruthenium complexes containing 4,4′-dicarboxy-2,2′-biquinoline (H_2dcbiq) and 5,8-dicarboxy-6,7-dihydrodibenzo[1,10]phenanthroline (H_2dcdh-

* To whom correspondence should be addressed. E-mail: sugihara-hideki@aist.go.jp. Phone: +81-29-861-4641. Fax: +81-29-861-6771.

(1) Nazeeruddin, M. K.; Kay, A.; Rodicio, I.; Humphry-Baker, R.; Müller, E.; Liska, P.; Vlachopoulos, N.; Grätzel, M. *J. Am. Chem. Soc.* **1993**, *115*, 6382−6390.
(2) Nazeeruddin, M. K.; Zakeeruddin, S. M.; Humphry-Baker, R.; Jirousek, M.; Liska, P.; Vlachopoulos, N.; Shklover, V.; Fischer, C.-H.; Grätzel, M. *Inorg. Chem.* **1999**, *38*, 6298−6305.
(3) Nazeeruddin, M. K.; Péchy, P.; Grätzel, M. *J. Chem. Soc., Chem. Commun.* **1997**, *18*, 1705−1706.
(4) Nazeeruddin, M. K.; Péchy, P.; Renouard, T.; Zakeeruddin, S. M.; Humphry-Baker, R.; Comte, P.; Liska, P.; Cevey, L.; Costa, E.; Shklover, V.; Spiccia, L.; Deacon, G. B.; Bignozzi, C. A.; Grätzel, M. *J. Am. Chem. Soc.* **2001**, *123*, 1613−1624.
(5) Islam, A.; Sugihara, H.; Yanagida, M.; Hara, K.; Fujihashi, G.; Tachibana, Y.; Katoh, R.; Murata, S.; Arakawa, H. *New J. Chem.* **2002**, *26*, 966−968.
(6) Sauvé, G.; Cass, M. E.; Coia, G.; Doig, S. J.; Lauermann, I.; Pomykal, K. E.; Lewis, N. S. *J. Phys. Chem. B* **2000**, *104*, 6821−6836.
(7) Islam, A.; Sugihara, H.; Hara, K.; Singh, L. P.; Katoh, R.; Yanagida, M.; Takahashi, Y.; Murata, S.; Arakawa, H. *J. Photochem. Photobiol., A* **2001**, *145*, 135−141.
(8) Licht, S. In *Encyclopedia of Electrochemistry*; Bard, A. J., Stratmann, M., Eds.; Wiley-VCH Verlag GmbH: Germany, 2002; Vol. 6, p 393−491.
(9) Nazeeruddin, M. K.; Müller, E.; Humphry-Baker, R.; Vlachopoulos, N.; Grätzel, M. *J. Chem. Soc., Dalton Trans.* **1997**, *23*, 4571−4578.
(10) Argazzi, R.; Bignozzi, C. A.; Heimer, T. A.; Castellano, F. N.; Meyer, G. J. *Inorg. Chem.* **1994**, *33*, 5741−5749.
(11) Heimer, T. A.; Heilweil, E. J.; Bignozzi, C. A.; Meyer, G. J. *J. Phys. Chem. A* **2000**, *104*, 4256−4262.
(12) Islam, A.; Hara, K.; Singh, L. P.; Katoh, R.; Yanagida, M.; Murata, S.; Takahashi, Y.; Sugihara, H.; Arakawa, H. *Chem. Lett.* **2000**, *5*, 490−491.
(13) Islam, A.; Sugihara, H.; Singh, L. P.; Hara, K.; Katoh, R.; Nagawa, Y.; Yanagida, M.; Takahashi, Y.; Murata, S.; Arakawa, H. *Inorg. Chim. Acta* **2001**, *322*, 7−16.
(14) Zakeeruddin, S. M.; Nazeeruddin, M. K.; Humphry-Baker, R.; Grätzel, M. *Inorg. Chim. Acta* **1999**, *296*, 250−253.
(15) Renouard, T.; Fallahpour, R.-A.; Nazeeruddin, M. K.; Humphry-Baker, R.; Gorelsky, S. I.; Lever, A. B. P.; Grätzel, M. *Inorg. Chem.* **2002**, *41*, 367−378.

10.1021/ic034674x CCC: $25.00
Published on Web 10/25/2003

Chart 1

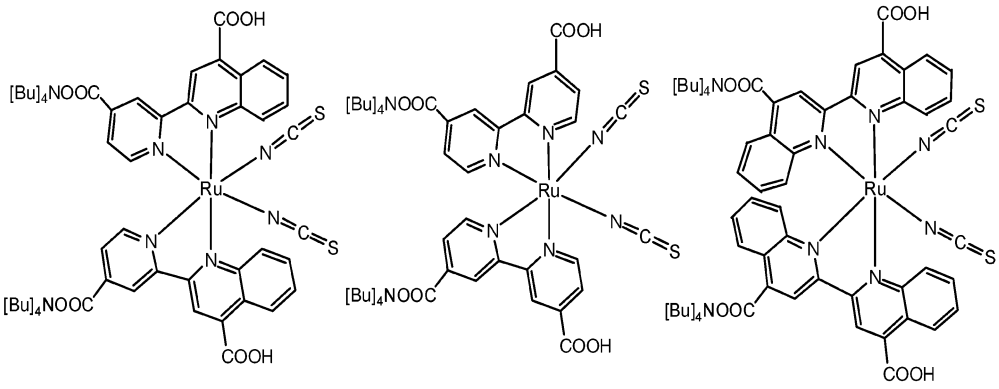

1 **2** **3**

ph).[12,13] Nanocrystalline TiO_2 solar cells sensitized with these complexes have a low solar energy conversion efficiency, because the lowest excited state of the ruthenium complex is less negative than the conduction band edge (E_{cb}) of TiO_2. Few improvements in the solar energy conversion efficiency of dye-sensitized solar cells have been obtained by tuning of the energy level of the excited state.[14,15] The quantum yield (ϕ_{inj}) of the charge injection is related to the free energy change ($-\Delta G_{inj}$), expressed as $-\Delta G_{inj} = E_{cb} - E_{Ru(III)/Ru(II)^*}$, where $E_{Ru(III)/Ru(II)^*}$ is the energy level of the excited state of the dye.[16,17] The relationship between the ϕ_{inj} value and ΔG_{inj} can be explained by taking into account the energy distribution of the E_{cb} value originating from the site heterogeneity.[17] Recently, Hoertz and co-workers proposed that the ligand-localized trapping site reduces the ϕ_{inj} value of solar cells based on nanocrystalline TiO_2 when the ruthenium complexes contain a ligand with a low-lying π^* orbital.[18]

We newly synthesized $[NBu_4]_2$[*cis*-Ru(Hdcpq)$_2$(NCS)$_2$] (**1**; NBu_4 = tetrabutylammonium, H_2dcpq = 4-carboxy-2-[2′-(4′-carboxypyridyl)]quinoline, see Chart 1). Complex **1** achieved efficient sensitization of nanocrystalline TiO_2 films over a wide visible and near-IR wavelength range, generating a large short-circuit photocurrent.[19,20] The ruthenium complex **1** adsorbed on TiO_2 was characterized by Raman and IR spectroscopy and electrochemistry. We compared the photovoltaic properties, such as the short-circuit photocurrent and the open-circuit photovoltage, of solar cells based on nanocrystalline TiO_2 sensitized with complex **1** with those of **2**- and **3**-sensitized solar cells.

Experimental Section

1. Materials. All materials were reagent grade and were used as received unless otherwise noted. $[NBu_4]_2$[*cis*-Ru(Hdcbpy)$_2$(NCS)$_2$] (**2**) was purchased from Solaronix S.A (Lausanne, Switzerland). $[NBu_4]_2$[*cis*-Ru(Hdcpq)$_2$(NCS)$_2$] (**1**) and $[NBu_4]_2$[*cis*-Ru(Hdcbiq)$_2$(NCS)$_2$] (**3**) were synthesized according to the literature.[13,19]

***cis*-[Ru(H_2dcpq)$_2$Cl$_2$].** Ru(Me_2SO)Cl_2 (Me_2SO = dimethyl sulfoxide) (0.33 g), H_2dcpq (0.41 g), and KCl (0.35 g) were dissolved in ethylene glycol. The mixture was heated near reflux for 30 min. After cooling, the solvent was evaporated completely. The solid was stirred for 2 h in 3 M HCl solution and then filtered on a membrane filter. After the solid was dissolved in methanol, most of the solvent was evaporated, and *cis*-[Ru(H_2dcpq)$_2$Cl$_2$] was precipitated with acetone. The yield was 0.43 g (81%). Electrospray ionization mass spectrum (ESI-MS): m/z 758 $(M - H^+)^-$, 378.5 $(M - 2H^+)^{2-}$, 252 $(M - 3H^+)^{3-}$. Anal. Calcd for $C_{32}H_{20}Cl_2N_4O_8Ru \cdot 2CH_3OH$: C, 49.52; H, 3.42; N, 6.79. Found: C, 49.16; H, 3.19; N, 6.40.

$[NBu_4]_2$[*cis*-Ru(Hdcpq)$_2$(NCS)$_2$] (1). ^{1}H NMR (400 MHz, CD_3OD) δ 1.00 (m, 12H), 1.35 (m, 8H), 1.60 (m, 8H), 3.20 (m, 8H), 6.69 (d, J = 9.0 Hz, 1H), 7.09 (t, J = 7.0 Hz, 1H), 7.48 (t, J = 7.0 Hz, 1H), 8.18 (d, J = 6.0 Hz, 1H), 8.58 (d, J = 9.0 Hz, 1H), 8.85 (s, 1H), 9.33 (s, 1H), 9.36 (d, J = 6.0 Hz, 1H).

2. Preparation of Samples. Dye-Sensitized TiO_2 Films. Nanocrystalline TiO_2 films were prepared as described earlier.[20−23] The geometric surface area of the TiO_2 film was 0.25 cm^2, and the thickness of the film was 18 μm. The actual inner surface of the TiO_2 film was estimated by BET measurement. The specific surface area of the nanocrystalline TiO_2 films was estimated to be 52 m^2 g^{-1}.[20] The density of the nanocrystalline TiO_2 film (2.1 g cm^{-3}) was calculated by measuring the weight of the nanocrystalline TiO_2 film (0.25 cm^2 × 18 μm). The roughness factor of the TiO_2 film (18 μm) was calculated to be 1970. The thickness of the films was measured with a Tencor Alpha Step 500 profiler. Transparent nanocrystalline TiO_2 films (thickness 3 μm) were used for the measurement of the absorbed photon-to-current conversion efficiency (APCE) spectra and the electrochemistry for ruthenium complexes adsorbed on the TiO_2. The bare TiO_2 films were dipped in ethanolic dye solution at a concentration of 3×10^{-4} M at room temperature for 20 h. The amount of adsorbed ruthenium complex (M_{ad}/mol) was determined by desorbing the complex from the TiO_2 film into a 0.01 M NaOH 1:1 (v/v) ethanol−water solution and measuring the absorption spectrum of the complex. The coverage (Γ) (mol cm^{-2}) was defined as $\Gamma = M_{ad}/0.25$.

(16) Asbury, J. B.; Hao, E.; Wang, Y.; Ghosh, H. N.; Lian, T. *J. Phys. Chem. B* **2001**, *105*, 4545−4557.
(17) Katoh, R.; Furube, A.; Hara, K.; Murata, S.; Sugihara, H.; Arakawa, H.; Tachiya, M. *J. Phys. Chem. B* **2002**, *106*, 12957−12964.
(18) Hoertz, P. G.; Thompson, D. W.; Friedman, L. A.; Meyer, G. J. *J. Am. Chem. Soc.* **2002**, *124*, 9690−9691.
(19) Yanagida, M.; Islam, A.; Tachibana, Y.; Fujihashi, G.; Katoh, R.; Sugihara, H.; Arakawa, H. *New J. Chem.* **2002**, *26*, 963−965.
(20) Yanagida, M.; Yamaguchi, T.; Kurashige, M.; Fujihashi, G.; Hara, K.; Katoh, R.; Sugihara, H.; Arakawa, H. *Inorg. Chim. Acta* **2003**, *351*, 283−290.
(21) Hara, K.; Sugihara, H.; Tachibana, Y.; Islam, A.; Yanagida, M.; Sayama, K.; Arakawa, H. *Langmuir* **2001**, *17*, 5992−5999.
(22) Hara, K.; Horiuchi, H.; Katoh, R.; Singh, L. P.; Sugihara, H.; Sayama, K.; Murata, S.; Tachiya, M.; Arakawa, H. *J. Phys. Chem. B* **2002**, *106*, 374−379.
(23) Sayama, K.; Sugihara, H.; Arakawa, H. *Chem. Mater.* **1998**, *10*, 3825−3832.

Table 1. Absorption, Luminescence, and Electrochemical Properties of Ruthenium Complexes **1**, **2**, and **3**

complex	absorption max/nm ($\epsilon/10^3$ dm^3 mol^{-1} cm^{-1})[a] MLCT band	emission (77 K)[b]		electrochemical properties (V) vs SCE[d]		
		λ_{max}/nm	E^{00}[c]/eV	$E_{Ru(III)/Ru(II)}$[e]	$E_{p,L/L^-}$[f]	$E_{Ru(III)/Ru(II)^*}$[g]
2	396 (13), 528 (14)	715	1.80	0.68	−1.12	−1.12
1	390 (sh, 8), 575 (13)	820	1.62	0.74	−0.99	−0.88
3	410 (sh, 9), 625 (12)	840	1.50	0.71	−0.91	−0.79

[a] Measured in ethanol. [b] Measured in ethanol−methanol (4:1 v/v) glass at 77 K. [c] E^{00} is estimated from a tangent to the high energy side of the corrected emission spectra at 77 K. [d] Measured in 0.1 M $LiClO_4$ acetonitrile solution. [e] Peak potential of the differential pulse voltammogram for ruthenium complexes bound to nanocrystalline TiO_2 film. [f] Reduction peak potential of ruthenium complexes adsorbed on F-SnO_2. [g] $E_{Ru(III)/Ru(II)^*} = E_{Ru(III)/Ru(II)} - E^{00}$.

Ruthenium-Complex-Adsorbed Fluorine-Doped SnO_2 (F-SnO_2). Ruthenium-complex-adsorbed fluorine-doped SnO_2 (F-SnO_2) (Nippon Sheet Glass Co.) electrodes were prepared to investigate the electrochemical properties of the ruthenium complex. The F-SnO_2 sheet was annealed at 500 °C and soaked in a solution of 3×10^{-4} M ruthenium complex for 72 h.

3. Methods. ^{1}H NMR spectra were recorded by a Varian INOVA 400 spectrometer. ESI-MS were measured with a Micromass QUATTRO II mass spectrometer. UV−vis spectra were measured with a Shimadzu UV3101PC spectrometer. Corrected emission spectra were obtained by using a Hitachi Co. F-4500 spectrophotometer. Spectra at 77 K were measured in 4:1 (v/v) ethanol−methanol glasses immersed in liquid N_2. All solutions were prepared to give an approximate concentration of 1×10^{-5} M. All samples for emission measurements were purged with an Ar stream. IR spectral measurements were performed with a Spectrum One (Perkin-Elmer) spectrometer with an attenuated total reflectance accessory (ZnSe prism) at a resolution of 4 cm^{-1}. The IR spectra of dyes adsorbed on TiO_2 were corrected for bare TiO_2. Resonance Raman spectra were measured on an NRS-1000 laser Raman spectrophotometer. A green diode laser (532 nm) provided the excitation source.

A Bioanalytical Systems BAS-100 electrochemical analyzer was used to perform cyclic voltammetry (CV) or differential pulse voltammetry (DPV). A conventional three-electrode system consisting of a platinum wire counter electrode, a ruthenium-complex-adsorbed F-SnO_2 or nanocrystalline TiO_2 film working electrode, and a Ag−AgCl (saturated aqueous KCl) reference electrode (NaCl salt bridge) was used for the electrochemical measurements. Electrode potential values were corrected to the saturated calomel electrode (SCE). Scan rates were 0.05−0.5 V s^{-1}. CV was carried out in 0.1 M $LiClO_4$−acetonitrile solution. Organic solvents (<0.005% water) and $LiClO_4$ were used as received (Wako Pure Chemical Industries).

Photoelectrochemical measurements were performed in a sandwich-type two-electrode cell consisting of a dye-coated TiO_2 film electrode, a polyethylene film spacer, an electrolyte solution, and a Pt film counter electrode. The electrolyte solution of the cell consisted of 0.6 M (1,2-dimethyl-3-propyl)imidazolium iodide, 0.05 M I_2, and 0.1 M LiI in acetonitrile. The concentration of I_3^- of this electrolyte solution was evaluated to be 49 mM from UV−vis spectra. The photovoltaic measurements were conducted by using a Xe lamp light source simulating the AM 1.5 spectrum (Wacom, WXS-80C-3, 100 mW cm^{-2}). The incident monochromatic photon-to-current conversion efficiency (IPCE) was measured by using a monochromatic Xe lamp (SX150C) source (CED99-W, Bunko Keisoku Co.). Thin and transparent nanocrystalline TiO_2 film (3 μm) electrodes were used for the absorbed monochromatic photon-to-current conversion efficiency (APCE) measurement. The dark current density−voltage ($J_{dark}-V$) measurement was performed on a Solartron Instruments model 1260 impedance/gain-phase analyzer linked to a Schlumberger Instruments model 1286 electrochemical interface. The scan rate was 0.02 V s^{-1}. The $J_{dark}-V$ curves were corrected for series resistance (R_{cell}) due mainly to the ohmic resistance of the F-SnO_2 in the cells.[6] The R_{cell} value of the cells was extracted from the high-frequency limits of the Bode plots of the cells and determined to be ca. 3−7 Ω. The corrected voltage, V_{corr}, was calculated from V, R_{cell}, and the dark current or photocurrent (I) by using the equation $V_{corr} = V - IR_{cell}$.

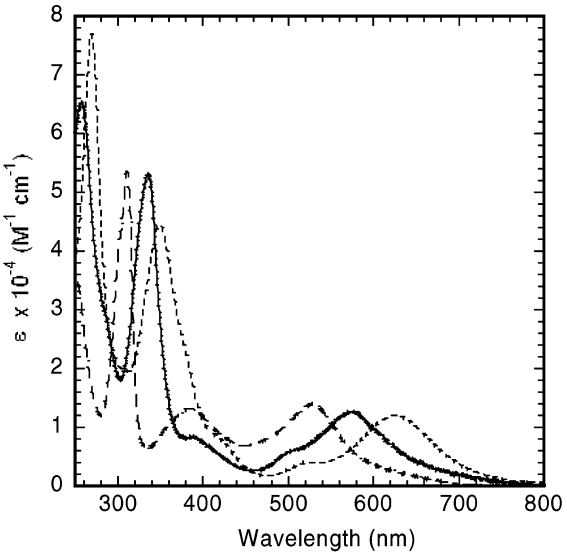

Figure 1. UV−vis absorption spectra of **1** (—), **2** (- - -), and **3** (···) in ethanol at room temperature.

Results and Discussion

1. Spectroscopic Properties. Relevant spectroscopic properties are summarized in Table 1, and the UV−vis absorption spectra are shown in Figure 1. The $\pi-\pi^*$ and lowest MLCT absorption bands were dependent on the π^* level of the complex. Emission maxima of **1**, **2**, and **3** at 77 K were at 820, 715, and 840 nm, respectively. The 0−0 transition energies (E^{00}) of **1**, **2**, and **3** were 1.62, 1.80, and 1.50 eV, respectively, as determined from a tangent to the high energy side of the corrected emission spectra. The E^{00} values of these complexes decreased in the order **2** > **1** > **3** owing to stabilization of the π^* orbital of the ligand. All absorption and emission spectra of partly protonated ruthenium complexes were blue shifted compared with those of fully protonated complexes.

The Raman and IR spectra of **2**, **1**, and **3** adsorbed on TiO_2 were measured to investigate the adsorption mode of the ruthenium complexes. The Γ values of **1**, **2**, and **3** adsorbed on TiO_2 were 1.8×10^{-7}, 2.1×10^{-7}, and 1.8×10^{-7} mol cm^{-2}, respectively. Assuming that each dye molecule occupies an area of 100 Å^2, the coverage of the ruthenium complexes on the TiO_2 surface is 60%.

Table 2. IR Bands (cm^{-1}) of Ruthenium Complexes **1**−**3** and Ruthenium Complexes Adsorbed on Nanocrystalline TiO_2[a]

assignment	complex	C−H stretch of NBu_4^+	C−N stretch of NCS	C═O stretch	symmetric stretch of COO^-	antisymmetric stretch of COO^-
2	solid	2960, 2934, 2873	2095	1693	1606	1352
	on TiO_2		2112	1722	1592	1376
1	solid	2960, 2934, 2873	2095	1707, 1668	1617	1325
	on TiO_2		2113	1729	1580	1390
3	solid	2960, 2934, 2873	2095	1704, 1665	1612	1332
	on TiO_2		2097	1723	1581	1408

[a] The IR spectra of complexes **2**, **1**, and **3** and complexes adsorbed on nanocrystalline TiO_2 are included in the Supporting Information.

Weak Raman signals of the NCS ligand for **2**, **1**, and **3** adsorbed on TiO_2 were observed at 2144, 2134, and 2148 cm^{-1}, respectively. The bands at 1487, 1554, and 1622 cm^{-1} are attributed to bipyridine skeletal vibrations of complex **2**. The bands at 1363, 1477, 1551, and 1618 cm^{-1} are ascribed to pyridylquinoline skeletal vibrations of complex **1**. The bands at 1369, 1471, 1544, and 1597 cm^{-1} are due to biquinoline skeletal vibrations of complex **3**. The broad bands at 1280, 1254, and 1240 cm^{-1} of **2**, **1**, and **3** are ascribed to the symmetric vibrations of carboxylate (COO^-).[24]

The IR spectra of complexes **1**, **2**, and **3** (solid samples) and these complexes adsorbed on nanocrystalline TiO_2 are summarized in Table 2. The IR spectra of dye molecules show intense bands at 2095 cm^{-1} ascribed to NCS stretching (N-bound from).[2,25−27] The IR spectra of **1**, **2**, and **3** adsorbed on nanocrystalline TiO_2 show the C−N stretching bands of NCS, the C═O stretching of the protonated carboxyl group (COOH), and the antisymmetric and symmetric stretching of the carboxylate (COO^-). The intensities of each peak for **1**, **2**, and **3** on TiO_2 corresponded to the Γ values. The energy difference between the antisymmetric (ν_{a,COO^-}) and the symmetric (ν_{s,COO^-}) stretching frequencies of the carboxyl groups was used to estimate the binding mode of the ruthenium complexes to the TiO_2 surface.[25,26] The energy differences ($\Delta = \nu_{a,COO^-} - \nu_{s,COO^-}$) for **1**, **2**, and **3** on TiO_2 were lower than those for the solid samples of the ruthenium complexes. Complexes **1**, **2**, and **3** were anchored via bidentate or bridging coordination to Ti^{4+} on the TiO_2 surface. The Raman and IR spectra of complexes **1**, **2**, and **3** and complexes adsorbed on nanocrystalline TiO_2 are included in the Supporting Information.

2. Electrochemical Properties of Ruthenium Complexes Adsorbed on TiO_2 or F-SnO_2. Cyclic voltammetry of complexes **1**, **2**, and **3** adsorbed on F-SnO_2 was conducted in 0.1 M $LiClO_4$ acetonitrile solution. Quasireversible curves due to the Ru(II)/Ru(III) redox reaction were observed at around 0.68 V versus SCE. The redox potentials ($E_{Ru(II)/Ru(III)}$'s) of **1**, **2**, and **3** on F-SnO_2 were 0.69, 0.66, and 0.68 V, respectively. The peak current of the Ru(II)/Ru(III) redox reaction varies linearly with the square root of the scan rate if the complex does not attach to F-SnO_2 and diffuses from the electrolyte solution to the electrode. However, the peak current of the Ru(II)/Ru(III) redox reaction for complexes **1**, **2**, and **3** on F-SnO_2 varied linearly with the scan rate (0.05−0.5 V s^{-1}), showing that complexes **1**, **2**, and **3** adsorb onto the surface of F-SnO_2.[28] Irreversible waves were observed when the scan rate was lower than 0.05 V s^{-1}. The integration of the anodic wave provides an estimate of the amounts of adsorbed molecules (Γ/mol cm^{-2}) for the apparent surface area of F-SnO_2. The Γ values of **1**, **2**, and **3** adsorbed on F-SnO_2 were 5.6×10^{-10}, 5.0×10^{-10}, and 5.7×10^{-10} mol cm^{-2}, respectively. The peak potential ($E_{p,L/L^-}$) for the first-ligand-based reduction of **1**, **2**, and **3** on F-SnO_2 was observed at −0.99, −1.12, and −0.91 V, respectively. The observed large current of the reduction peak can be attributed to the irreversible multireduction of a ligand. Cyclic voltammograms of **1**, **2**, and **3** on F-SnO_2 are included in the Supporting Information.

The electrochemical properties of the ruthenium complexes adsorbed on TiO_2 were investigated in 0.1 M $LiClO_4$ acetonitrile solution by cyclic voltammetry.[29−36] Typical cyclic voltammograms for ruthenium complexes **1**, **2**, and **3** on TiO_2 (3 μm) are shown in Figure 2. The electrode potential was swept negatively at first. The hysteretic shape between 0 and −0.95 V versus SCE has been ascribed to electron accumulation/discharge on the nanocrystalline film.[32,34−36] The current (i) at values more negative than 0 V can be described by following equation

$$i = dQ/dt = C(dE/dt) \quad (1)$$

where Q is the electric charge (C), t is time (s), C is the capacitance (F) and dE/dt is the scan rate (V s^{-1}). The peak potential for the reduction of **1**, **2**, and **3** on TiO_2 was not observed under this condition.

Quasireversible curves between 0.4 and 0.9 V are attributed to the Ru(II)/Ru(III) redox reaction of complexes

(24) Zakeeruddin, S. M.; Nazeeruddin, M. K.; Humphry-Baker, R.; Grätzel, M. *Inorg. Chem.* **1998**, *37*, 5251−5259.
(25) Finnie, K. S.; Bartlett, J. R.; Woolfrey, J. L. *Langmuir* **1998**, *14*, 2744−2749.
(26) Bauer, C.; Boschloo, G.; Mukhtar, E.; Hagfeldt, A. *J. Phys. Chem. B* **2002**, *106*, 12693−12704.
(27) Belser, P.; Zelewsky, A. V. *Helv. Chim. Acta* **1980**, *63*, 1675−1702.
(28) Bard, A. J.; Faulkner, L. R. *Electrochemical Methods: Fundamentals and Applications*; Wiley-Interscience: NewYork, 1980.
(29) Heimer, T. A.; D'Arcangelis, S. T.; Farzad, F.; Stipkala, J. M.; Meyer, G. J. *Inorg. Chem.* **1996**, *35*, 5319−5324.
(30) Kelly, C. A.; Farzad, F.; Thompson, D. W.; Stipkala, J. M.; Meyer, G. J. *Langmuir* **1999**, *15*, 7047−7054.
(31) Trammell, S. A.; Meyer, T. J. *J. Phys. Chem. B* **1999**, *103*, 104−107.
(32) Fabregat-Santiago, F.; Mora-Seró, I.; Garcia-Belmonte, G.; Bisquert, J. *J. Phys. Chem. B* **2003**, *107*, 758−768.
(33) Zaban, A.; Meier, A.; Gregg, B. A. *J. Phys. Chem. B* **1997**, *101*, 7985−7990.
(34) van de Lagemaat, J.; Park, N.-G.; Frank, A. J. *J. Phys. Chem. B* **2000**, *104*, 2044−2052.
(35) Wang, H.; He, J.; Boschloo, G.; Lindström, H.; Hagfeldt, A.; Lindquist, S.-E. *J. Phys. Chem. B* **2001**, *105*, 2529−2533.
(36) Willis, R. L.; Olson, C.; O'Regan, B.; Lutz, T.; Nelson, J.; Durrant, J. R. *J. Phys. Chem. B* **2002**, *106*, 7605−7613.

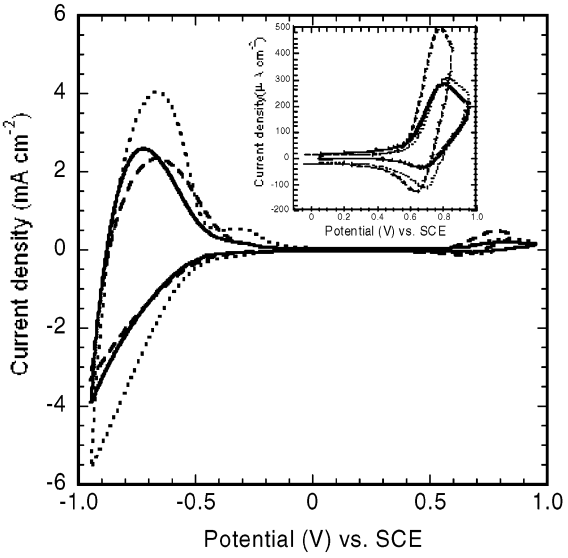

Figure 2. Cyclic voltammograms of complexes **1** (—), **2** (- - -), and **3** (···) adsorbed on nanocrystalline TiO_2 electrodes in 0.1 M $LiClO_4$ acetonitrile solution. Inset shows cyclic voltammograms for the Ru(II)/Ru(III) redox reaction of complexes **1**, **2**, and **3** adsorbed on TiO_2 film. Scan rate was 0.5 V s^{-1}.

1, **2**, and **3** on TiO_2 film, which are shown in the inset of Figure 2. The anodic peak potentials of **1**, **2**, and **3** on TiO_2 were 0.82, 0.79, and 0.80 V, respectively. The cathodic peak potentials of **1**, **2**, and **3** on TiO_2 were 0.67, 0.63, and 0.69 V, respectively. The peak currents of the Ru(II)/Ru(III) redox reaction for complexes **1**, **2**, and **3** on TiO_2 varied linearly with the scan rate (0.2−0.5 V s^{-1}).[29,30] The peak potentials of the differential pulsed voltammogram for **1**, **2**, and **3** on TiO_2 were 0.74, 0.68, and 0.71 V, respectively, which were close to the $E_{Ru(II)/Ru(III)}$ values of complexes **1**, **2**, and **3** on F-SnO_2. The Γ values of complexes **1**, **2**, and **3** on TiO_2 were 1.2×10^{-8}, 2.5×10^{-8}, and 1.6×10^{-8} mol cm^{-2}, respectively, estimated by measuring the absorption spectra after desorbing each complex from the TiO_2 film into a 0.01 M NaOH 1:1 (v/v) ethanol−water solution. The Γ values of complexes **1**, **2**, and **3** on TiO_2, estimated by the integration of the anodic current density, were 1.5×10^{-9}, 2.2×10^{-9}, and 1.8×10^{-9} mol cm^{-2}, respectively, values which were ca. 3.5 times larger than the Γ values of complexes **1**, **2**, and **3** on F-SnO_2. These results show that complexes **1**, **2**, and **3** on TiO_2 are also electrochemically oxidized and reduced. On the other hand, the Γ values estimated by the integration of the anodic current density were ca. 90% smaller than the Γ values estimated by desorbing the complex from the TiO_2 film into a NaOH solution. The $E_{Ru(II)/Ru(III)}$ value and the current due to the redox reaction were independent of the thickness (3−18 μm) of the TiO_2 films. The Ru(II)/Ru(III) redox reaction of the ruthenium complexes on nanocrystalline TiO_2 occurs only on the TiO_2 film adjacent to the F-SnO_2. These results can be explained by the electron transfer among ruthenium complexes adsorbed on TiO_2.[31]

The characteristic shape of the cyclic voltammograms was observed at a more negative potential than 0 V. The shapes of the cyclic voltammograms of complexes **1**, **2**, and **3** on TiO_2 differed from each other. According to the equivalent circuit of TiO_2/redox electrolyte solution, the accumulation layer of the trap state on TiO_2 is in series with Helmholtz layer.[32−34] The current has been ascribed to accumulation of the electric charge to the trap state on TiO_2 since the capacitance of trap sites (C_{ts}) is much smaller than Helmholtz capacitance (C_H) at more negative potential than 0 V.[32,34−36] The charge (Q_a) estimated from the integration of the anodic current density for complexes **1**, **2**, and **3** on the TiO_2 electrode was 1.56×10^{-3}, 1.59×10^{-3}, and 2.52×10^{-3} C cm^{-2}, respectively. The Q_a was linearly correlated with the Γ values. The potentials −0.5 and −0.9 V, which bracket the potential range in which the charge/discharge current of **1** and **3** adsorbed on TiO_2 electrodes was observed, corresponded to the $E_{p,L/L^-}$ values of complexes **1** and **3**, respectively, on the F-SnO_2 electrode. These results show that complexes **1** and **3** on TiO_2 became the trap sites for an injected electron in the conduction band of TiO_2 (see discussion in the next section). If the Q_a value corresponds to the number of trap sites (N_t), the N_t values for complexes **1**, **2**, and **3** adsorbed on the TiO_2 electrode are 1.0×10^{16}, 1.0×0^{16}, and 1.6×10^{16} cm^{-2}, corresponding to 134%, 66%, and 164%, respectively, of the Γ values estimated by desorbing the complexes from the TiO_2 film into a NaOH solution. If we assume that all the trap sites of **2** adsorbed on the TiO_2 electrode are composed of intrinsic defects of TiO_2, the N_t values for **1** and **3** adsorbed on TiO_2 can be estimated to be 68% and 98% of the Γ values, respectively. We assumed the accumulation layer is in parallel with the ruthenium complex layer on TiO_2. The number of trap sites for **1** adsorbed on TiO_2 is ca. 30% lower than the Γ value. The energetic depth (ΔE) of trap sites is defined as $\Delta E = E_{p,L/L^-} - E_{cb}$. If $\Delta E < 0$, the complex does not act as an electron trap. But if $\Delta E > 0$, the complex acts as an electron trap. The $E_{p,L/L^-}$ value of **1** on F-SnO_2 was very close to the E_{cb} value, as shown in the next section. Because the ΔE value varies with the energy distribution of the E_{cb} value as a result of variations in the morphology of the surface of the nanocrystalline metal oxide semiconductor,[17] not all of ruthenium complex **1** adsorbed on the TiO_2 may act as an electron trap.

3. Photovoltaic Performance. Quantum Yields of Charge Injections from Ruthenium Complexes to TiO_2. The energetics of the interface between nanocrystalline TiO_2 sensitized with complex **1**, **2**, or **3** and electrolyte solution containing iodide anion (I^-) as an electron donor is described schematically in Figure 3. The redox potential ($E_{1/2}(I^-/I_3^-)$) of I^-/I_3^- and the E_{cb} value were 0.30 and −0.80 V reported by Myung et al. and Liu et al., respectively.[37,38] The $E_{Ru(II)/Ru(III)}$ values of **1**, **2**, and **3** were comparable. Because the E^{00} values decreased in the order **2** > **1** > **3**, the Ru(III)/Ru(II) redox potential ($E_{Ru(III)/Ru(II)^*}$) of the excited ruthenium complex shifted positively in the order **2**, **1**, and **3**.

The performance of complexes **1**, **2**, and **3** as sensitizers on nanocrystalline TiO_2 is summarized in Table 3. Typical photocurrent density−photovoltage curves of **1**-, **2**-, and **3**-sensitized solar cells are shown in Figure 4. The short-circuit photocurrent density (J_{sc}) of **1**-sensitized nanocrys-

(37) Myung, N.; Licht, S. *J. Electrochem. Soc.* **1995**, *142*, L129−L132.
(38) Liu, G.; Jaegermann, W.; He, J.; Sundström, V.; Sun, L. *J. Phys. Chem. B* **2002**, *106*, 5814−5819.

Table 3. Amount of Ruthenium Complexes **1**, **2**, and **3** Adsorbed Per Square Centimeter of Geometrical Surface Area and Photovoltaic Performance in Electrolyte Solution with or without 4-*tert*-Butylpyridine (TBP) under AM 1.5 Illumination (100 mW cm^{-2})

		without TBP[b]				with 0.5 M TBP			
complex	Γ[a] (10^{-7} mol cm^{-2})	J_{sc} (mA cm^{-2})	V_{oc} (V)	ff[c] (%)	η[c] (%)	J_{sc} (mA cm^{-2})	V_{oc} (V)	ff (%)	η (%)
2	2.1	17.7	0.52	64	5.9	15.3	0.71	73	7.9
1	1.8	15.1	0.48	68	4.9	5.6	0.56	77	2.4
3	1.8	4.8	0.35	68	1.2	1.1	0.44	73	0.4

[a] The amount of adsorbed ruthenium complex was determined by desorbing it from TiO_2 film into a 0.01 M NaOH 1:1 (v/v) ethanol−water solution and measuring its absorption spectrum. [b] The electrolyte solution was composed of 0.6 M (1,2-dimethyl-3-propyl)imidazolium iodide, 0.05 M I_2, and 0.1 M LiI in acetonitrile. [c] ff and η are the fill factor and the overall efficiency, respectively.

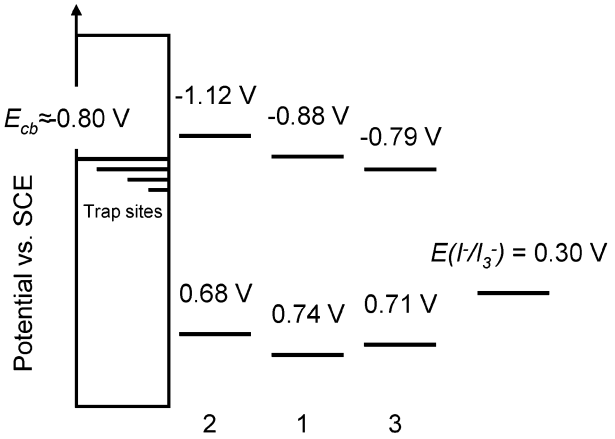

Figure 3. Schematic of the energetics of the interface between an I^-/I_3^- electrolyte solution and nanocrystalline TiO_2 sensitized with **1**, **2**, and **3**.

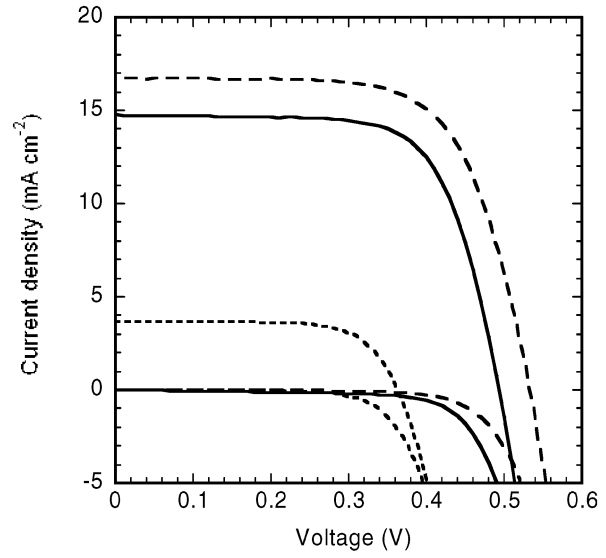

Figure 4. Photocurrent density−photovoltage characteristics of **1**-sensitized (—), **2**-sensitized (- - -), and **3**-sensitized (·····) solar cells based on nanocrystalline TiO_2. The onset of the dark current densities for **1**-sensitized (—), **2**-sensitized (- - -), and **3**-sensitized (···) solar cells are also shown.

talline TiO_2 solar cells was comparable with that of **2**-sensitized solar cells. Although complex **3** had a wide spectral response, it showed low photocurrent densities. The IPCE spectra of nanocrystalline TiO_2 solar cells sensitized with **1**, **2**, and **3** are shown in Figure 5. The IPCE is defined as

$$\mathrm{IPCE}(\lambda) = \frac{hc}{q\lambda}\left(\frac{J_{sc}(\lambda)}{I(\lambda)}\right) \times 10^6 = \mathrm{APCE}(\lambda) \times \mathrm{LHE}(\lambda) \quad (2)$$

where I, h, c, q, and λ are the irradiation power (W cm^{-2}),

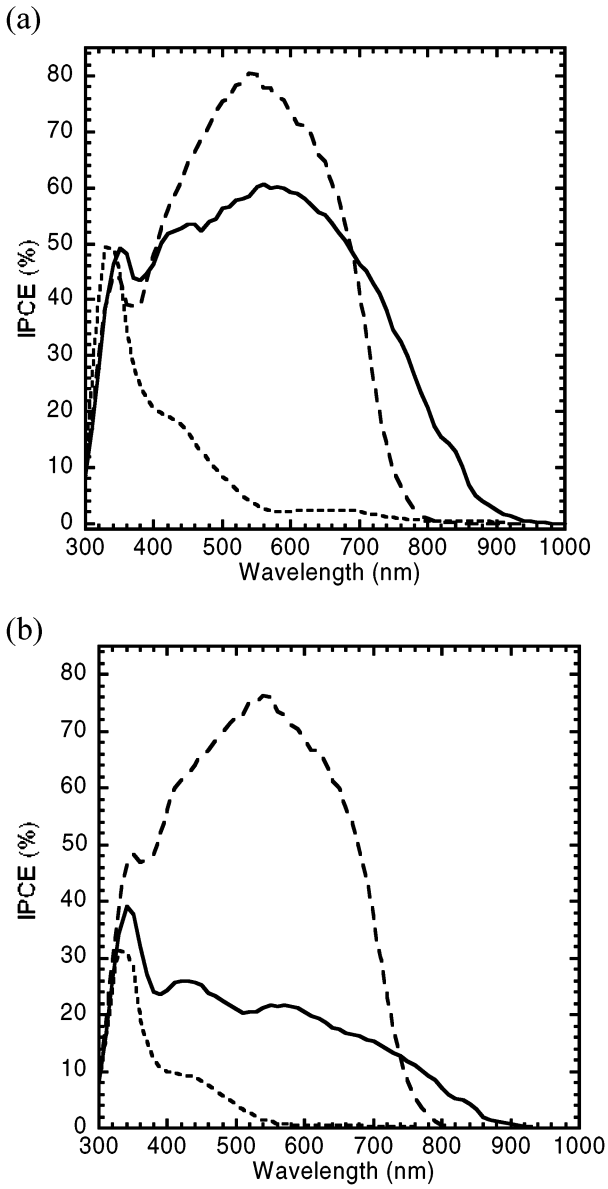

Figure 5. Photocurrent action spectra for **1**-sensitized (—), **2**-sensitized (- - -), and **3**-sensitized (···) solar cells based on nanocrystalline TiO_2. The incident photon-to-current conversion efficiency (IPCE) is plotted as a function of wavelength. (a) The electrolyte solution was composed of 0.6 M (1,2-dimethyl-3-propyl)imidazolium iodide, 0.05 M I_2, and 0.1 M LiI in acetonitrile. (b) The electrolyte solution was composed of 0.6 M (1,2-dimethyl-3-propyl)imidazolium iodide, 0.05 M I_2, 0.1 M LiI, and 0.5 M 4-*tert*-butylpyridine (TBP) in acetonitrile.

Planck's constant (J s), the speed of light in a vacuum (m s^{-1}), the quantity of charge on the electron (C), and the wavelength (nm), respectively.[1] LHE(λ) and APCE(λ) are

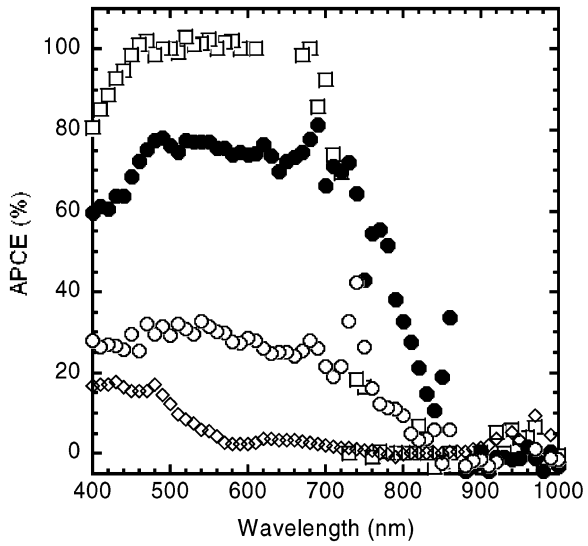

Figure 6. Absorbed photon-to-current conversion efficiency (APCE) spectra for **1**-sensitized (●), **2**-sensitized (□), and **3**-sensitized (◇) solar cells based on nanocrystalline TiO_2. The electrolyte solution was composed of 0.6 M (1,2-dimethyl-3-propyl)imidazolium iodide, 0.05 M I_2, and 0.1 M LiI in acetonitrile. The APCE spectrum for the **1**-sensitized (○) solar cell in the electrolyte containing 0.5 M TBP is also shown.

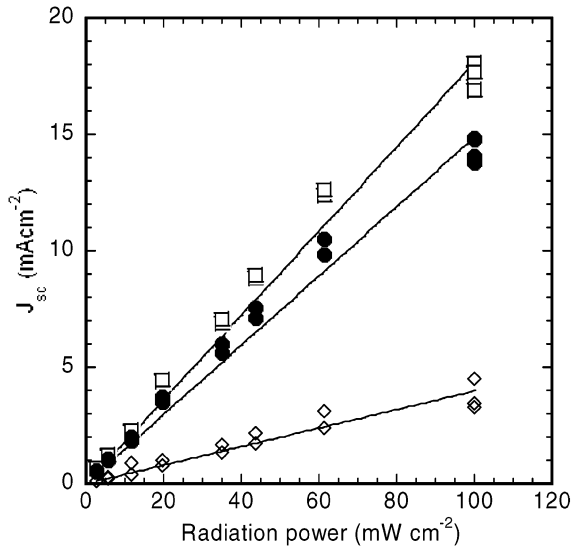

Figure 7. Radiant power dependence of the short-circuit photocurrent density (J_{sc}) for **1**-sensitized (●), **2**-sensitized (□), and **3**-sensitized (◇) solar cells. The electrolyte solution was composed of 0.6 M (1,2-dimethyl-3-propyl)imidazolium iodide, 0.05 M I_2, and 0.1 M LiI in acetonitrile.

the light harvesting efficiency and the absorbed photon-to-current conversion efficiency at each wavelength, respectively. The LHE(λ) is defined as

$$\mathrm{LHE}(\lambda) = 1 - 10^{-\mathrm{ABS}(\lambda)} \tag{3}$$

where ABS(λ) is absorbance of ruthenium complex adsorbed on nanocrystalline TiO_2. Figure 5a shows that the **1**-sensitized solar cell was effectively photosensitized over a large portion of the solar spectrum from 400 to 900 nm. However, the IPCE maximum for the **1**-sensitized solar cell was 20% lower than that of the **2**-sensitized solar cell. The APCE values for the **1**-, **2**-, and **3**-sensitized solar cells based on transparent nanocrystalline TiO_2 (3 μm) were shown in Figure 6. The APCE values at 610 nm for the **1**-, **2**-, and **3**-sensitized solar cells were 74%, 100%, and 3%, respectively. The APCE value decreased in the order **2** > **1** > **3**.

Figure 7 shows that the J_{sc} values of **1**-, **2**-, and **3**-sensitized TiO_2 solar cells (18 μm thickness) varied in direct proportion to the radiant power (AM 1.5, 3.25−100 mW cm^{-2}). The photocurrent density (J_{ph}) is given by[39]

$$J_{ph} = J_{inj} - J_r \tag{4}$$

where J_{inj} is the electron injection current density resulting from dye sensitization and J_r is the reverse current density. The electron injection rate constants for any sensitizers have been reported to be very large (>10^{13} s^{-1}).[16,17] The intensity of signal for the time-resolved transient absorption of electrons corresponds to the IPCE value. Electron transfers from TiO_2 to I_3^- or the oxidized dye are much slower than electron injection from the dye to TiO_2 at short circuit. Assuming that the J_r value can be neglected at short circuit, the J_{sc} value (A cm^{-2}) is defined as

$$J_{inj} \approx J_{sc} = q\phi AI \tag{5}$$

The ϕ value corresponds to the APCE value under illumination of solar light. A is given by

$$A \approx \frac{10^{-6}}{I_0 hc}\int_0^\infty \mathrm{LHE}(\lambda) I_0(\lambda) \lambda \, \mathrm{d}\lambda \tag{6}$$

where $I_0(\lambda)$ is the irradiation power (W cm^{-2} nm^{-1}) at the wavelength for a solar light (I_0 = 100 mW cm^{-2}). The slopes in Figure 7 for **1**-, **2**-, and **3**-sensitized solar cells were 0.15, 0.18, and 0.04 V^{-1}, respectively. The equation ABS(λ) = 1000 $\epsilon\Gamma$ was used to estimate the A value. The ϵ is the extinction coefficient in Figure 1, and the Γ values of **1**-, **2**-, and **3**-sensitized solar cells are 1.8 × 10^{-7}, 2.1 × 10^{-7}, and 1.8 × 10^{-7} mol cm^{-2}, respectively. The A values for **1**-, **2**-, and **3**-sensitized solar cells were 1.21 × 10^{18}, 1.06 × 10^{18}, and 1.28 × 10^{18} J^{-1}, respectively. The ϕ values of **1**-, **2**-, and **3**-sensitized solar cells were estimated to be ca. 80%, 100%, and 20%, respectively. Assuming that the E_{cb} value is independent of the kind of sensitizers on TiO_2, the $-\Delta G_{inj}$ values of **1**-, **2**-, and **3**-sensitized solar cells were 0.08, 0.32, and −0.01 eV, respectively. The relationship between ϕ or APCE value at 610 nm and $-\Delta G_{inj}$ is shown in Figure 8. The ϕ value gradually decreased with the decrease in $-\Delta G_{inj}$.[17,40] In other words, the ϕ values depend on the $E_{Ru(III)/Ru(II)^*}$ values. The IPCE maximum, APCE maximum, and ϕ value are indices of the efficiency of electron injection (ϕ_{inj}), respectively.[16,17] The relationship between ϕ_{inj} and $-\Delta G_{inj}$ has been explained by taking into account the energy distribution of the E_{cb} value originating from the site heterogeneity of TiO_2 electrode.[17]

(39) Huang, S. Y.; Schlichthörl, G.; Nozik, A. J.; Grätzel, M.; Frank, A. J. *J. Phys. Chem. B* **1997**, *101*, 2576−2582.

(40) Hara, K.; Sato, T.; Katoh, R.; Furube, A.; Ohga, Y.; Shinpo, A.; Suga, S.; Sayama, K.; Sugihara, H.; Arakawa, H. *J. Phys. Chem. B* **2003**, *107*, 597−606.

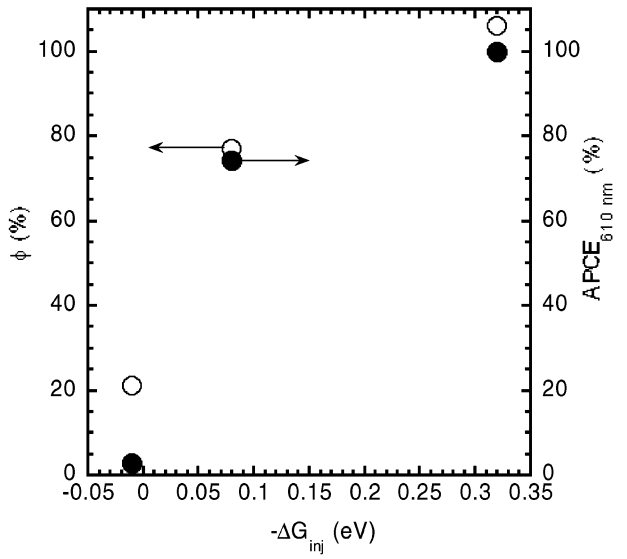

Figure 8. The ϕ and APCE values at 610 nm for **1**-, **2**-, and **3**-sensitized solar cells, plotted as functions as $-\Delta G_{inj} = E_{cb} - E_{Ru(III)/Ru(II)^*}$.

The open-circuit photovoltage (V_{oc}) of solar cells sensitized with **1**, **2**, and **3** increased when 4-*tert*-butylpyridine (TBP) was added into an electrolyte because TBP is regarded as a blocking agent of reverse electron transfer and shifts the E_{cb} value more negatively (Table 2).[39,41] The IPCE maximum and the APCE maximum of **1**-, **2**-, and **3**-sensitized solar cells in the visible region decreased with the addition of TBP to the electrolyte because the $-\Delta G_{inj}$ value decreased (Figures 5b and 6). With the addition of TBP to the electrolyte, the IPCE maximum of **1**-, **2**-, and **3**-sensitized solar cells using an electrolyte without TBP decreased by 40%, 4%, and 10%, respectively. The E_{cb} value shifted negatively by ca. 0.1 V, as calculated from the increase of the V_{oc} values with the addition of TBP. The $-\Delta G_{inj}$ value of the **1**-sensitized solar cell is 0.24 eV smaller than that of the **2**-sensitized solar cell because the $E_{Ru(III)/Ru(II)^*}$ of complex **1** is more positive than that of complex **2**. The decrease of the IPCE maximum of the **1**-sensitized solar cell was 10 times larger than that of the **2**-sensitized solar cell when the $-\Delta G_{inj}$ value decreases by 0.1 eV. These results show that the energy level of the excited state of complex **1** is a marginal value for efficient sensitization.

Reverse Electron Transfer from TiO_2 to I_3^- in the Dark. The V_{oc} values of dye-sensitized solar cells decreased in the order **2** > **1** > **3** with increasing dark current density (J_{dark}) (Figure 4). When the dark current density−electrode potential ($J_{dark}-E$) curves of **1**-, **2**-, and **3**-sensitized TiO_2 electrodes in I^-/I_3^- electrolyte were measured, the onset of the potential for large dark current density shifted positively in the order of **3**, **1**, and **2**, corresponding to the dark current density−voltage ($J_{dark}-V$) curve (see Supporting Information). The increase in dark current results from the increase in the electron transfer from TiO_2 to I_3^-, represented by the net reaction

$$2e^- + I_3^- \rightarrow 3I^- \qquad \text{(I)}$$

The decrease of V_{oc} values in the order **2** > **1** > **3** can be explained by reverse electron transfer from TiO_2 to I_3^- through the ruthenium complexes on TiO_2. Electron transfer to the electrolyte is followed by reduction of the ruthenium complex, as shown:

$$e^-(TiO_2) + \textit{cis}\text{-}[RuL_2(NCS)_2]/TiO_2 \xrightarrow{k_{b1}} \textit{cis}\text{-}[RuL(L^{\cdot -})(NCS)_2]/TiO_2 \qquad \text{(II)}$$

$$\textit{cis}\text{-}[RuL(L^{\cdot -})(NCS)_2]/TiO_2 + I_2 \xrightarrow{k_{b2}} \textit{cis}\text{-}[RuL_2(NCS)_2]/TiO_2 + I_2^- \qquad \text{(III)}$$

The ruthenium complex in the ground state traps the electron in TiO_2 under forward bias (TiO_2 is at a more negative potential than the $E_{1/2}(I^-/I_3^-)$ value). The trapped electrons on the ruthenium complex react with I_2.[39] Under steady-state conditions, the amount of *cis*-[$RuL(L^{\cdot -})(NCS)_2$]/TiO_2 as an occupied trap site (Γ_R) follows:

$$d\Gamma_R/dt = k_{b1}(N - N_0)\Gamma_t - k_{b2}\Gamma_R C_{ox} = 0 \qquad (7)$$

where N is excess electron density, N_0 is electron density in the dark, Γ_t is the amount of *cis*-[$RuL_2(NCS)_2$]/TiO_2 as an unoccupied trap site, and C_{ox} is the concentration of I_2. J_{dark} is described as

$$J_{dark} = qk_{b1}(N - N_0)\Gamma_t = qk_{b2}\Gamma_R C_{ox} \qquad (8)$$

The total amount of molecules as trap sites (Γ') is constant.

$$\Gamma' = \Gamma_t + \Gamma_R \qquad (9)$$

The Γ' value can be defined as

$$\Gamma' = \theta\Gamma \qquad (10)$$

where θ is constant for a ruthenium complex on TiO_2. From eqs 7−10, J_{dark} is described as

$$J_{dark} = \frac{qk_{b1}k_{b2}C_{ox}\theta\Gamma(N - N_0)}{k_{b2}C_{ox} + k_{b1}(N - N_0)} \qquad (11)$$

The concentration of C_{ox} in the electrolyte is much larger than the N value. We assumed that the k_{b1} value is comparable to the k_{b2} value. If $k_{b2}C_{ox} \gg k_{b1}(N - N_0)$, then J_{dark} can be written as

$$J_{dark} = qk_{b1}\theta\Gamma(N - N_0) \qquad (12)$$

As the redox species such as I_3^- and I^- tend to interact with polypyridyl ligand of metal complexes,[42] the k_{b2} value may be also larger than the k_{b1} value.

The excess electron density is exponentially related to the external voltage (V) of the solar cell by the equation[43]

$$N = N_0 \exp(qV/(\gamma kT)) \qquad (13)$$

(41) Schlichthörl, G.; Huang, S. Y.; Sprague, J.; Frank, A. J. *J. Phys. Chem. B* **1997**, *101*, 8141−8155.
(42) Walter, B. J.; Elliott, C. M. *Inorg. Chem.* **2001**, *40*, 5924−5927.
(43) Södergren, S.; Hagfeldt, A.; Olsson, J.; Lindquist, S.-E. *J. Phys. Chem.* **1994**, *98*, 5552−5556.

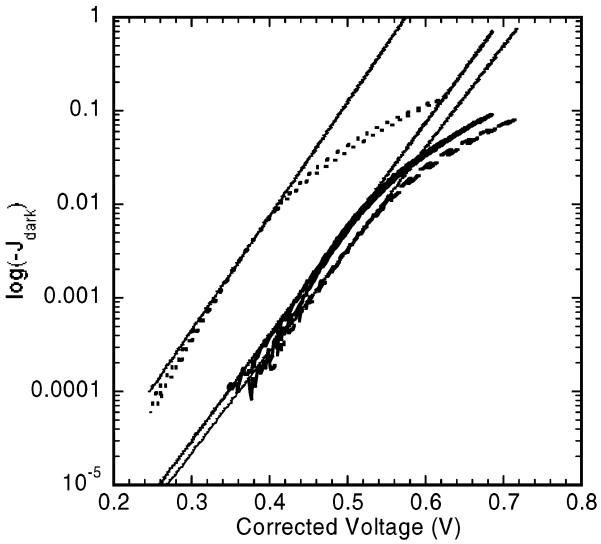

Figure 9. Dark current density-corrected voltage ($\log(-J_{dark}) - V$) characteristics of **1**-sensitized (—), **2**-sensitized (- - -), and **3**-sensitized (··· ·) solar cells in electrolyte solution composed of 0.6 M (1,2-dimethyl-3-propyl)imidazolium iodide, 0.05 M I_2, and 0.1 M LiI in acetonitrile.

where k, γ, and T are the Boltzmann constant, an ideality factor, and the absolute temperature, respectively. Thus, J_{dark} can be written as

$$J_{dark} = J_{dark,0}\{\exp(qV/(\gamma kT)) - 1\} \quad (14)$$

$$J_{dark,0} = qk_{b1}\theta\Gamma N_0 \quad (15)$$

The $J_{dark}-V$ behaviors of **1**-, **2**-, and **3**-sensitized TiO_2 solar cells, of which the Γ values are 1.8×10^{-7}, 1.5×10^{-7}, and 1.8×10^{-7} mol cm^{-2}, respectively, are shown in Figure 9. The current density above -2×10^{-3} A cm^{-2} was scattered. The negative deviation from linear at large applied bias is due to the mass transfer of I_3^- in the porous structure or other reverse electron transfer from TiO_2 to the electrolyte. Any artificial variations in $J_{dark,0}$ and γ were minimized by choosing similar current densities (-2×10^{-3} to -5×10^{-3} A cm^{-2}). The slopes of the semilogarithmic plots for **1**-, **2**-, and **3**-sensitized TiO_2 solar cells shown in Figure 9 were 82, 92, and 88 mV/decade, respectively. The γ value corresponds to the ideality factor of the diode. The γ values of **1**-, **2**-, and **3**-sensitized TiO_2 solar cells were 1.39, 1.56, and 1.49, respectively, corresponding to the values reported by Huang et al. and Dloczik et al.[39,44] The γ value depends on the charge collection barrier at the F-SnO_2/TiO_2 interface, the electron transfer across the TiO_2/redox electrolyte interface, and potential drops such as the double layer at the TiO_2/redox electrolyte interface, and the Nernstian shift caused by the diffusion limitation of redox couples at high current density.[43,45] The $J_{dark,0}$ values of **1**-, **2**-, and **3**-sensitized TiO_2 solar cells estimated from eq 15 were 1.2×10^{-8}, 1.2×10^{-8}, and 9.8×10^{-8} A cm^{-2}, respectively. The N_t values for complexes **1**, **2**, and **3** adsorbed on the TiO_2 electrode are 134%, 66%, and 164% of the Γ values, respectively. If the θ values for **1**-, **2**-, and **3**-sensitized TiO_2 solar cells are assumed to be 0.8, 0.5, and 1, respectively, the $k_{b1}N_0$ value of **1**-, **2**-, and **3**-sensitized TiO_2 solar cells are 0.9×10^{-6}, 1.7×10^{-6}, and 5.6×10^{-6}, respectively. The $k_{b1}N_0$ value of the **1**-sensitized TiO_2 solar cell was comparable to that of the **2**-sensitized TiO_2 solar cell. The $k_{b1}N_0$ value of the **3**-sensitized TiO_2 solar cell was clearly the largest of the three.

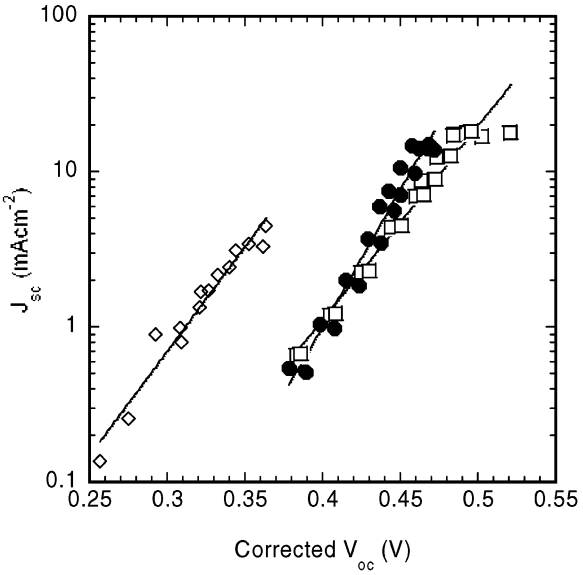

Figure 10. Radiant power dependence of the open-circuit photovoltage (V_{oc}) for **1**-sensitized (●), **2**-sensitized (□), and **3**-sensitized (◊) solar cells. The electrolyte solution was composed of 0.6 M (1,2-dimethyl-3-propyl)-imidazolium iodide, 0.05 M I_2, and 0.1 M LiI in acetonitrile.

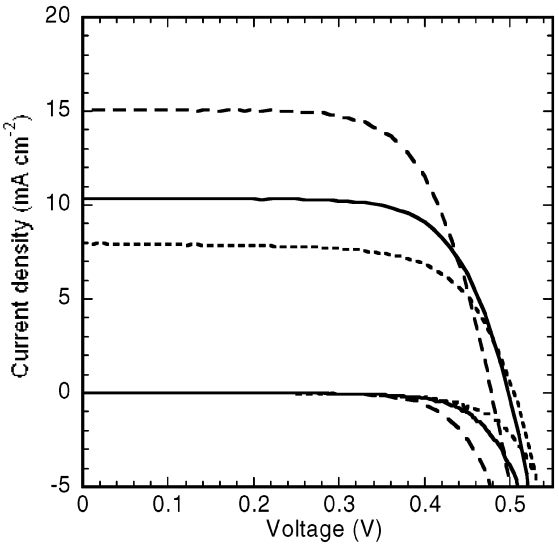

Figure 11. Photocurrent density−photovoltage characteristics depended on the coverage (Γ) of ruthenium complex **1** adsorbed on TiO_2. The Γ values are 1.7×10^{-7} (- - -), 0.97×10^{-7} (—), and 0.44×10^{-7} mol cm^{-2} (···). The onset of the dark current density is also shown.

Reverse Electron Transfer from TiO_2 to I_3^- under Illumination. The relationship between the J_{sc} and V_{oc} values for **1**-, **2**-, and **3**-sensitized TiO_2 solar cells is shown in Figure 10 for varying radiant power. The V_{oc} values were corrected for R_{cell}. Assuming that $J_{dark} = J_r$ at open circuit under

(44) Dloczik, L.; Ileperuma, O.; Lauermann, I.; Peter, L. M.; Ponomarev, E. A.; Redmond, G.; Shaw, N. J.; Uhlendorf, I. *J. Phys. Chem. B* **1997**, *101*, 10281−10289.
(45) Fajardo, A. M.; Lewis, N. S. *J. Phys. Chem. B* **1997**, *101*, 11136−11151.

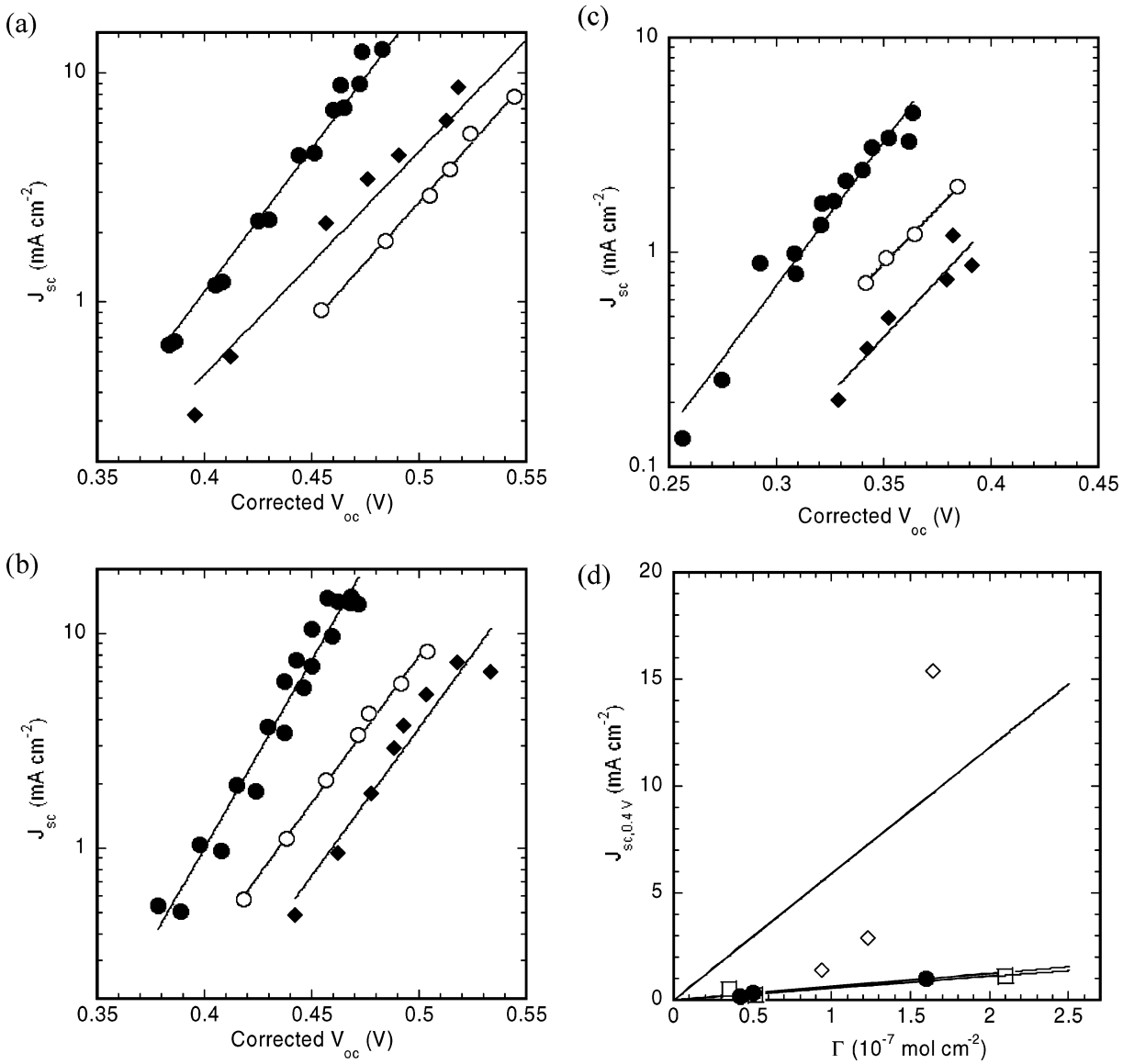

Figure 12. Radiant power dependence of the open-circuit photovoltage (V_{oc}) for **1**-, **2**-, and **3**-sensitized solar cells. (a) Plots of log J_{sc} vs V_{oc} for the **2**-sensitized solar cell. The Γ values are 2.1×10^{-7} (●), 0.52×10^{-7} (○), and 0.35×10^{-7} mol cm^{-2} (♦). (b) Plots of log J_{sc} vs V_{oc} for the **1**-sensitized solar cell. The Γ values are 1.60×10^{-7} (●), 0.50×10^{-7} (○), and 0.42×10^{-7} mol cm^{-2} (♦). (c) Plots of log J_{sc} vs V_{oc} for the **3**-sensitized solar cell. The Γ values are 1.64×10^{-7} (●), 1.23×10^{-7} (○), and 0.94×10^{-7} mol cm^{-2} (♦). (d) Calculated J_{sc} value ($J_{sc,0.4V}$) at $V_{oc} = 0.4$ V vs Γ value for **1**-sensitized (●), **2**-sensitized (□), and **3**-sensitized (◊) solar cells. The $J_{sc,0.4V}$ value was extrapolated from the line of fit of the relationship between the J_{sc} and V_{oc} values, as shown in Figure 12a−c.

illumination, from eqs 5, 14, and 15, we obtain[39]

$$V_{oc} = \frac{\gamma kT}{q} \ln\left(\frac{\phi AI}{k_{b1}\theta\Gamma N_0} + 1\right) \tag{16}$$

If $\phi_{inj}AI \gg k_{b1}\Gamma N_0$, we obtain

$$V_{oc} \approx \frac{\gamma kT}{q} \ln\left(\frac{\phi AI}{k_{b1}\theta\Gamma N_0}\right) = \frac{\gamma kT}{q} \ln\left(\frac{J_{sc}}{J_{dark,0}}\right) \tag{17}$$

Equation 17 describes the dependence of V_{oc} on the irradiation power, the Γ value, and the k_{b1} value. The slopes of the semilogarithmic plots for **1**-, **2**-, and **3**-sensitized TiO_2 solar cells (Figure 10) were 58, 81, and 71 mV/decade, respectively. The γ values for **1**-, **2**-, and **3**-sensitized TiO_2 solar cells were 0.98, 1.36, and 1.20, respectively. The $J_{dark,0}$ values of **1**-, **2**-, and **3**-sensitized TiO_2 solar cells were 1.0×10^{-5}, 1.7×10^{-5}, and 3.0×10^{-7} A cm^{-2}, respectively. The $J_{dark,0}$ value of the **1**-sensitized TiO_2 solar cell was comparable to that of the **2**-sensitized TiO_2 solar cell. The γ and $J_{dark,0}$ values were different from the values estimated from the $J_{dark}-V$ curve. The $J_{dark,0}$ value under illumination was larger than that in the dark. The oxidized ruthenium complex is produced after an electron injection under illumination. Our model did not consider reverse electron transfer from TiO_2 to the oxidized dye at a high concentration of I^-, because the oxidized dye is immediately reduced by I^-. However, I^- may not fully diffuse in mesoporous TiO_2. Reverse electron transfer from TiO_2 to the oxidized dye may increase the $J_{dark,0}$ value under illumination.[33,46]

(46) Dittrich, T.; Beer, P.; Koch, F.; Weidmann, J.; Lauermann, I. *Appl. Phys. Lett.* **1998**, *73*, 1901−1903.

Effect of the Amount of Adsorption of Ruthenium Complexes on the Solar Cell. The dependence of a typical photocurrent density−photovoltage curve of a **1**-sensitized solar cell on the Γ value is shown in Figure 11. The J_{sc} value decreased because of the low LHE value when the Γ value decreased; in contrast, the V_{oc} value increased.[6] When the Γ value increased, the onset of electrode potential for the dark current density shifted positively at the $J_{dark}-E$ curve measurement, corresponding to the $J_{dark}-V$ curve shown in Figure 11. According to eq 17, the V_{oc} value shifts ca. 59 mV/decade for the Γ value, corresponding to the shift of V_{oc} in Figure 11. The radiation power dependent V_{oc} values for **1**-, **2**-, and **3**-sensitized TiO_2 solar cells under various Γ values were shown in Figure 12a−c. The slopes of the semilogarithmic plots for **1**-, **2**-, and **3**-sensitized TiO_2 solar cells were independent of the Γ values. The intercept on the V_{oc} axis for **1**-, **2**-, and **3**-sensitized TiO_2 solar cells shifted ca. 40−100 mV/decade for the Γ value, corresponding to eq 17. The intercept on the J_{sc} axis also depended on the Γ values. The $J_{dark,0}$ value is linearly correlated with Γ from eq 15. The relationship between the calculated J_{sc} value at $V_{oc} = 0.4$ V ($J_{sc,0.4V}$) and Γ is shown in Figure 12d. The $J_{sc,0.4V}$ value was extrapolated from the line of fit of the relationship between the J_{sc} and V_{oc} values when the radiant power changed from 3.25 to 100 mW cm^{-2}. The slope of the plot in Figure 12d corresponds to the k_{b1} value under irradiation. The V_{oc} value of the **1**-sensitized solar cell was smaller than that of the **2**-sensitized solar cell (Table 2). These results show that the k_{b1} value of the **1**-sensitized solar cell was slightly larger than that of the **2**-sensitized solar cell, and also that the k_{b1} value of the **3**-sensitized solar cell was much larger than that of the **1**- and **2**-sensitized solar cells.

Conclusion

$[NBu_4]_2$[*cis*-$Ru(Hdcpq)_2(NCS)_2$] (**1**) was newly synthesized, and its spectral and electrochemical properties were compared with those of $[NBu_4]_2$[*cis*-$Ru(Hdcbpy)_2(NCS)_2$] (**2**) and $[NBu_4]_2$[*cis*-$Ru(Hdcbiq)_2(NCS)_2$] (**3**).

The photovoltaic performance of the solar cell based on TiO_2 sensitized with **1** was compared with those of the **2**- and **3**-sensitized solar cells. Complex **1** achieved an efficient sensitization of nanocrystalline TiO_2 films over a wide visible and near-IR wavelength range, generating a large short-circuit photocurrent. The IPCE maxima of **1**-, **2**-, and **3**-sensitized solar cells decreased in the order **2** > **1** > **3**. The IPCE maxima of **1**-sensitized solar cells changed dramatically with the addition of TBP. The energy level of the excited state of complex **1** is the marginal value for effective electron injection in dye-sensitized TiO_2 solar cells.

The V_{oc} values of dye-sensitized solar cells decreased in the order **2** > **1** > **3** with the increase of the dark current resulting from reverse electron transfer from TiO_2 to I_3^-. The cyclic voltammetry for **1**-, **2**-, and **3**-adsorbed TiO_2 electrodes in 0.1 M $LiClO_4$ acetonitrile solution indicated that the number of trap sites increased in the order **2** < **1** < **3** as the $E_{p,L/L^-}$ values of these complexes on F-SnO_2 shifted positively. We consider that the injected electron is trapped in the ground state of the ruthenium complex and reacts with I_3^- under open-circuit conditions under illumination. This model can explain the dependence of V_{oc} on the ruthenium complex, the radiant power, and the Γ value.

Acknowledgment. This work was supported by the New Energy and Industrial Technology Development Organization (NEDO) under the Ministry of Economy, Trade, and Industry (METI) of Japan.

Supporting Information Available: Raman spectra of complexes **1**−**3** adsorbed on TiO_2, IR absorption spectra of the dye powders for **1**−**3** and the complexes adsorbed on TiO_2, cyclic voltammograms of **1**−**3** adsorbed on F-SnO_2, and dark current density−potential curves of **1**−**3** adsorbed on TiO_2. This material is available free of charge via the Internet at http://pubs.acs.org.

IC034674X